

<https://doi.org/10.1038/s41522-025-00865-w>

# Emergent roles of infant gut microbes during the utilization of human milk oligosaccharides



Tomás Pröschle-Donoso<sup>1</sup>, Romina Díaz<sup>1</sup>, Javiera Vásquez-Dean<sup>1</sup>, Kineret Serebrinsky-Duek<sup>1</sup>, Ignacio Pezoa-Soto<sup>2</sup>, Alberto J. M. Martín<sup>2,3</sup> & Daniel Garrido<sup>1</sup> ✉

*Bifidobacterium* spp. are representative species of the infant gut microbiome. Human milk oligosaccharides (HMOs) are complex carbohydrates in breast milk, guiding gut microbiome assembly by establishing complex microbial interactions. Here, a synthetic community of seven infant gut microbes was subjected to single species dropouts in bioreactors using three HMOs. Substrate use, acid production, biomass, and metatranscriptomics revealed that *B. bifidum* was critical for degradation product formation and supporting cross-feeding. Removing *B. longum* subsp. *infantis*, known for intracellular HMO use, accelerated global growth and HMO consumption, suggesting competitive interactions. Some dropouts led to the accumulation of sialic acid, fucose, or lactose. Metatranscriptomics showed niche expansion, upregulated central metabolism and cross-feeding dependencies when certain species were removed. Modeling highlighted that HMO degradation rates strongly influence community dynamics. Overall, this study identifies key ecological roles in infant gut microbes and deepens our understanding of how HMOs shape microbiota assembly and function.

The intestinal microbiome plays a fundamental role in human health, especially during infancy, contributing to child nutrition and development, protecting against pathogens, and educating the immune system<sup>1</sup>. The composition of the infant gut microbiome changes dynamically during the first year of life<sup>2,3</sup>, being clearly different from the adult gut microbiome as it transitions to a mature state after the introduction of solid foods<sup>2,4</sup>.

Human milk is the gold standard for infant nutrition and provides a mixture of nutrients and bioactive components that support proper infant growth<sup>5,6</sup>. One hallmark of human breast milk is a high concentration of human milk oligosaccharides (HMOs)<sup>7</sup>, which, among other functions, shape the infant gut microbiome<sup>8,9</sup>. HMOs are a family of linear and branched unconjugated glycans composed of a lactose core with linear chains varying from 3 to 15 units. HMOs are composed of five monosaccharides: glucose, galactose, fucose, N-acetylglucosamine (GlcNAc), and N-acetylneuraminic acid (NeuAc; sialic acid)<sup>5,10</sup>. The proportions of fucosylated, sialylated, and non-fucosylated neutral HMOs in breast milk are 35–50%, 12–14%, and 42–55% respectively<sup>11</sup>. Some of the most abundant and representative HMOs are 2'-fucosyllactose (2'FL), lacto-N-tetraose (LNT), and 3'-sialyllactose (3'SL)<sup>11</sup>. Breastfeeding often enriches *Bifidobacterium* spp., though this varies across infants and populations<sup>5,12,13</sup>. These bacteria are beneficial for the host through diverse mechanisms<sup>14</sup>. The

ecological success of these microorganisms in the infant gut may be related to the overrepresentation of several carbohydrate utilization genes in their genomes, participating in the transport and metabolism of different types of HMOs<sup>15–18</sup>. Individual members of other taxa, such as *Lachnospiraceae* and *Bacteroides*, have also been described for their adaptation to HMO utilization<sup>19–21</sup>, while certain *Lactobacillus* strains exhibit limited growth on specific HMO substructures<sup>22</sup>.

The most studied species capable of metabolizing HMOs are *Bifidobacterium bifidum*, *Bifidobacterium longum* subsp. *infantis* (*B. infantis*), *Bifidobacterium longum* subsp. *longum* (*B. longum*) and *Bifidobacterium breve*, among others<sup>23,24</sup>. For example, *B. infantis* targets most HMOs and possesses multiple genes associated with transport via ABC transporters and enzymes that metabolize them intracellularly<sup>23,25</sup>. In contrast, *B. bifidum* can also grow on all types of HMOs but by an extracellular mechanism characterized by multiple membrane glycosyl hydrolases capable of breaking the glycosidic bonds in HMOs and transporting a few molecules such as lactose and lacto-N-biose<sup>26–28</sup>. *B. breve* and *B. longum* generally consume only certain HMO types, such as LNT, by an intracellular mechanism<sup>10,29</sup>. These different utilization strategies could have ecological implications, as an extracellular mechanism could favor carbohydrate cross-feeding, for example, of NeuAc or fucose<sup>30</sup>. HMO fermentation usually results in high

<sup>1</sup>Department of Chemical and Bioprocess Engineering, School of Engineering, Pontificia Universidad Católica de Chile, Av. Vicuña Mackenna, Santiago, Chile.

<sup>2</sup>Laboratorio de Redes Biológicas, Centro Científico y Tecnológico de Excelencia Ciencia & Vida, Fundación Ciencia & Vida, Santiago, Chile. <sup>3</sup>Escuela de Ingeniería, Facultad de Ingeniería, Arquitectura y Diseño, Universidad San Sebastián, Santiago, Chile. ✉e-mail: dgarridoc@ing.puc.cl

concentrations of acetate and lactate, which could also participate in cross-feeding interactions with butyrate and propionate producers<sup>30,31</sup>. In addition, *Bifidobacterium* and other species with similar nutritional niches targeting the same HMOs are expected to compete for some of these HMOs.

The role of individual species in the gut microbiome should be considered in the context of the collective activity of numerous microorganisms and their metabolites<sup>32</sup>. Metabolic interactions are highly frequent in the human gut microbiome, and metabolites participate in complex networks of cross-feeding or exploitative competition<sup>32,33</sup>. Understanding complex microbial ecosystems is crucial for predicting the functional state of the human gut microbiome and developing effective microbiome modulation strategies, for example, using HMOs<sup>34–37</sup>. Synthetic microbial communities assembled from host-derived strains have received considerable attention for the characterization of the ecological and metabolic features of the human gut microbiome<sup>38–40</sup>. Common approaches in microbe-microbe interactions combine 16S rRNA gene-based composition analysis with metabolite measurements, mathematical modeling, and metatranscriptomics. These methods collectively enable the examination of community dynamics, stability, inter-species metabolic interactions, and trophic roles within the microbiome. Controlled in vitro models can provide insights into microbe-specific temporal dynamics, niche overlap, and trophic interaction networks, shedding light on the coexistence of essential intestinal microbes in a competitive and dynamic ecosystem<sup>41–44</sup>.

This study aimed to determine functional and ecological roles within a synthetic microbial consortium, including important microorganisms with different mechanisms of HMO utilization, using a species dropout approach.

## Results

In this study, we assembled a synthetic consortium composed of seven infant gut microbes to determine their ecological roles during the consumption of HMO (Fig. 1). These microbes display different mechanisms of HMO utilization: some are well known for their ability to use multiple HMOs either intra or extracellularly (*B. infantis*, *B. bifidum*) or are partial HMO-utilizers (*B. breve*, *Bacteroides thetaiotaomicron*). Other species can use HMO-derived monosaccharides, such as fucose, sialic acid, GlcNAc, or lactose (*Escherichia coli*, *Pediococcus acidilactici*, *Lachnospirillum*

*symbiosum*). Table 1 presents additional functional and genomic information on these microorganisms. Synthetic consortia were cultured in batch bioreactors with a mixture of LNT, 2' FL, and 3' SL, and fermentations were assessed by growth kinetics, relative abundance of species, HMO consumption, acid production, and changes in community gene expression. Specific dropouts are indicated by a  $\Delta$  notation (e.g.,  $\Delta$ BBIF), indicating that the aforementioned species was omitted from the bioreactor (Table 1).

## Growth kinetics

We first evaluated how individual species dropouts affected growth parameters such as growth rate, total biomass, and lag time (Fig. 2). For the ALL consortium, the lag phase lasted 7.8 h, and  $\mu_{\max}$  was  $0.76 \text{ h}^{-1}$ . Growth rates were significantly reduced in the absence of *B. bifidum*, *B. breve*, and *P. acidilactici*, indicating these bacteria might contribute to the system's combined growth (Fig. 2). Absence of *P. acidilactici* significantly increased lag phase.  $\Delta$ BBIF had a lower growth rate and the shortest lag phase duration (Fig. 2).  $\Delta$ BINF and  $\Delta$ BTHE showed similar kinetic parameters to ALL, with an exponential phase starting earlier at 4 h. These results suggest that the absence of certain bacteria reduces community growth rate and total biomass, and some dropouts could accelerate the start of the exponential phase.

## Relative abundance of species

The microbial composition of the bioreactors was determined during the exponential and stationary growth phases by qPCR. This information could reveal how the absence of certain microbes allows others to expand their niche or affect the whole system due to their functional relevance. In the ALL consortium, *B. breve* dominated during the exponential phase, and *B. bifidum* during the stationary phase (Fig. 3). Both bacteria maintained a significant abundance across all conditions evaluated. The representation of *B. bifidum* increased earlier in the fermentation in the absence of *B. infantis* or *B. thetaiotaomicron* ( $\Delta$ BINF or  $\Delta$ BTHE; Fig. 3), suggesting competition. In contrast, the only condition in which *B. infantis* was dominant was in  $\Delta$ BBIF. In this condition, a higher representation of *E. coli* and *L. symbiosum* was found compared to ALL. In aggregate, the relative abundance analysis suggests possible scenarios of resource competition between dominant HMO users such as *B. bifidum*, *B. infantis*, or *B. thetaiotaomicron*. When controlling for differences in initial cell counts ( $\log_{10}$  fold change in absolute

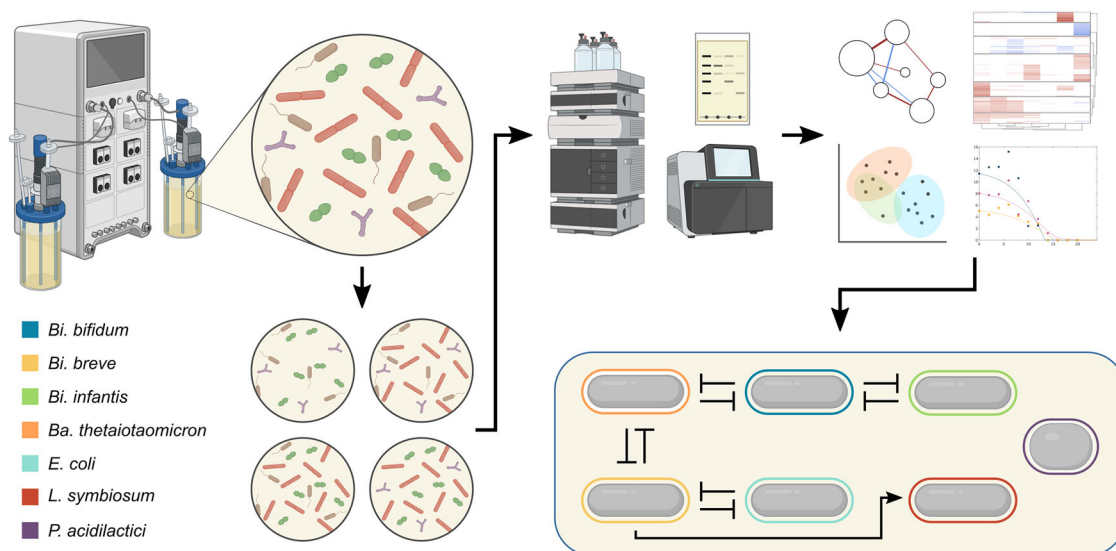


**Fig. 1 | Schematic summary of approaches used in this study.** Graphical abstract of the study. A biological replication of a synthetic consortium of seven infant gut microbes using three HMOs was established. Specific bacterial species were selectively removed, and the system was characterized by culture growth, metabolite production, and HMO utilization. Metatranscriptome analyses were obtained for each condition. Multivariate analyses and correlation networks were

obtained. Finally, a mathematical model consisting of a system of ordinary differential equations was constructed to quantify the degradation rates of complex sugars and enable comparisons across different experiments. These comprehensive analyses led to the development of a model describing interactions among the consortium's diverse bacterial members. Figures were retrieved from BioRender.

**Table 1 | Culture, functional, and genomic information of the microorganisms used in this study**

Microorganism	Dropout experiment	Culture medium	Culture collection	Functional and genomic evidence for HMO utilization	References
<i>Bifidobacterium bifidum</i> JCM 1254	ΔBBIF	MRS-cys	UCD	Utilizes LNT, 2'FL, 3'SL	91–93
<i>Bifidobacterium infantis</i> ATCC 15697	ΔBINF	MRS-cys	UCD	Utilizes LNT, 2'FL, 3'SL	50,94–96
<i>Bifidobacterium breve</i> 11	ΔBBRE	MRS-cys	This study	Predicted to consume LNT, fucose, NeuAc, and GlcNAc Alpha-L-fucosidase (EC 3.2.1.51); Sialidase (EC 3.2.1.18); N-acetylmannosamine kinase; N-acetylmannosamine-6-phosphate 2-epimerase; N-acetylmannosamine-6-phosphate 2-epimerase; lactaldelyde reductase; L-fucose mutarotase; L-fucose-proton symporter; L-fucosate dehydratase; PTS system N-acetylglucosamine-specific EIIICBA component; N-acetyl-D-glucosamine kinase; N-acetylglucosamine repressor; Glucosamine-6-phosphate deaminase	97–99
<i>Bacteroides thetaiotaomicron</i> VPI 5482	ΔBTHE	RCM	ATCC	Utilizes LNT, 2'FL, 3'SL	100,101
<i>Lachnospirillum symbiosum</i> WAL 14673	ΔLSYM	RCM	BEI resources	Predicted to consume NeuAc and release GlcNAc Beta-N-acetylhexosaminidase; sialic acid-binding periplasmic protein siaP; N-acetylglucosamine-6-phosphate 2-epimerase; N-acetylneuraminase	19
<i>Escherichia coli</i> K-12	ΔECOL	LB	UCD	Consumes fucose, NeuAc, and GlcNAc	102–104
<i>Pediococcus acidilactici</i> PT22	ΔPACI	MRS	This study	Predicted to consume fucose, NeuAc, and GlcNAc Alpha-L-fucosidase (EC 3.2.1.51); Sialic acid-specific 9-O-acetyl/esterase; Sialic acid utilization regulator, RqIR family; N-acetylneuraminase; N-acetylmannosamine kinase; N-acetylmannosamine-6-phosphate 2-epimerase; N-acetylglucosamine-6-phosphate deacetylase; Phosphoglucosamine mutase; Glucosamine-6-phosphate deaminase	

abundances; Supplementary Table 1), *B. bifidum* was able to increase up to 100 times its relative abundance in most dropouts, and *L. symbiosum* increased 600 times in ΔBBIF from its initial abundance.

**HMO consumption and metabolite production analysis**

It is likely that the absence of certain species changes HMO consumption patterns of this community, for example consumption times, preference for some HMO, or generation of degradation products. Similarly, short-chain fatty acids (SCFAs) could be differentially produced due to changes in HMO consumption or species abundances. Different patterns of HMO consumption were observed upon species dropouts (Fig. 4). Lactose was found to be present in one of the HMOs (3'SL), which was confirmed by TLC. The ALL condition showed a reduction in all HMO at 12 h, which resulted in fucose accumulation at the end of the experiment (Fig. 4). A gradual increase in lactose was observed up to 10 h, which can be explained by the extracellular degradation of 2'FL and 3'SL. In ΔBBIF, no free monosaccharides were found, and a gradual lactose increase was not observed. This is consistent with *B. bifidum* extracellular HMO hydrolysis and the release of degradation products (Fig. 4).

Interestingly, ΔBINF and ΔBTHE displayed accelerated degradations of all HMOs (up to 4–6 h) and an increase in monosaccharide release (fucose, galactose, and glucose), which were eventually consumed at 10–12 h (Fig. 4). This faster consumption is consistent with the HMO extracellular utilization mechanism of *B. bifidum* and suggests less competition, allowing *B. bifidum* to dominate earlier the consortium (Fig. 3). The absence of *B. breve*, *P. acidilactici*, or *L. symbiosum* caused a delay in monosaccharide removal that lasted until the end of the fermentation (Fig. 4). Finally, sialic acid concentrations in ALL bioreactors peaked at the exponential phase (Supplementary Fig 1), decreasing later, suggesting that some species consumed this monosaccharide. Dropouts of *B. breve*, *P. acidilactici*, and especially *L. symbiosum* resulted in the accumulation of sialic acid, suggesting they are responsible for NeuAc consumption.

Acetate and lactate were present at high concentrations as end products (Supplementary Fig 2). ΔBBIF resulted in the highest acetate concentration, and ΔBINF resulted in the highest lactate concentration. The absence of *B. breve* resulted in high succinate production by the consortium (Supplementary Fig 2), which correlates with an overabundance of *B. thetaiotaomicron*.

**Correlation analysis of bioreactor data**

Next, data from bioreactor kinetics, relative abundance, carbohydrate consumption, and acid production was used to determine if some variables of these systems showed non-evident correlations. Principal component analysis and a correlation matrix were calculated (Fig. 5). PCA indicated that the combined characteristics of ΔBTHE and ΔBINF dropouts were very similar. The ALL and ΔECOL bioreactors were unique and not grouped with other dropouts in the exponential phase (Fig. 5A), and ΔBBRE did not group with other dropouts in the stationary phase (Fig. 5B). Figure 5C shows that at the exponential phase, *B. bifidum* abundance correlated significantly with NeuAc and lactate concentrations, suggesting it contributes to their accumulation. In this phase, the concentrations of the three HMOs correlated positively, indicating that they are consumed at a similar rate (Fig. 5C). At the stationary phase, *B. thetaiotaomicron* correlated with succinate, indicating it contributes to its production, and *B. bifidum* with biomass production, which is consistent with its dominance across most conditions. The concentration of simple carbohydrates such as lactose, glucose, and lactose, instead of intact HMO, correlated positively at the stationary phase. This is consistent with the extensive release of simple carbohydrates after HMO degradation (Fig. 5B).

**Metatranscriptomic changes upon species dropouts**

We later aimed to determine global changes in gene expression in these synthetic consortia in exponential phase upon species dropouts, by metatranscriptomic RNA-seq (Supplementary Fig 3 and Fig. 6). Global gene expression during exponential phase of the ALL consortium was used as a

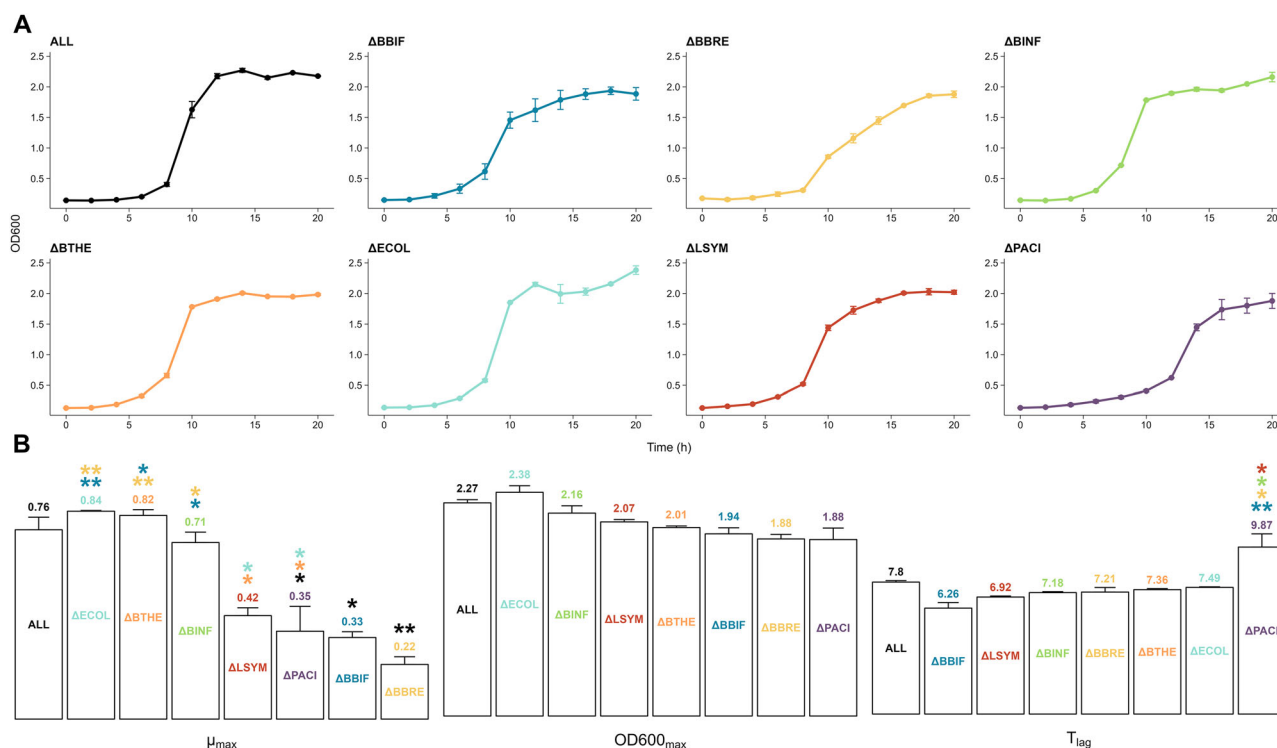


**Fig. 2 | Growth kinetics parameters in species dropout experiments.** Growth curves from the dropout experiments (A) and statistical analysis of their parameters (B). Culture growth was quantified by measuring OD<sub>600max</sub>. Growth curves were adjusted to the Gompertz-Zwietering growth model to determine its parameters for each experiment. The parameters μ<sub>max</sub> associated with the maximum growth rate,

OD<sub>600max</sub> associated with the maximum growth achieved, and T<sub>lag</sub> associated with lag phase time were analyzed. Statistical significance is reported based on adjusted *p*-values, and the color code indicates the experiment to which it differs. For instance, for the T<sub>lag</sub> parameter, two blue asterisks are observed over the ΔPACI experiment, indicating a significant difference compared to the ΔBBIF experiment (0.001 < \*\* < 0.01 < \* < 0.05).

reference, and Supplementary Table 2 presents the statistics of this analysis. After quality filtering, reads aligning with specific genes were counted and normalized. A PCA of the normalized counts matrix was used to compare replicates and determine metatranscriptional variations upon species dropouts (Supplementary Fig 3). ΔECOL had the most distinct metatranscriptome compared to other samples, followed by ΔBBIF. A heatmap of global gene expression across dropouts showed a large expansion in gene expression of *B. infantis* and *B. breve* in the absence of *B. bifidum*, suggesting a negative interaction between these bacteria. *E. coli* appeared the most responsive bacteria to any dropout (Fig. 6). In turn, *B. infantis*, *B. breve*, *B. bifidum* and *B. thetaiotaomicron* showed important changes in gene expression upon the absence of *E. coli* (Fig. 6). Finally, *B. thetaiotaomicron* presented several transcriptional changes when *B. breve* was not present, and *P. acidilactici* repressed several genes when *B. infantis*, *B. thetaiotaomicron* or *L. symbiosum* were left out (Fig. 6).

We next examined specific functional changes in the metatranscriptomes upon species dropouts. The most consistent changes mapped to genes related to the utilization of HMO-derived monosaccharides such as fucose, sialic acid, GlcNAc, and galactose, central metabolism and certain physiological functions (Supplementary Information). Two general patterns emerged: niche expansion under competitive release and dependence on cross-feeding partners.

In ΔBBIF, *B. infantis* and *B. breve* markedly upregulated several HMO transport and degradation genes (LNB/GNB clusters, type 2 HMO utilization cluster, fucosidases, sialidases), together with fermentative pathways for GlcNAc, galactose, fucose, and NeuAc. Similar induction patterns were observed in ΔBINF, where *B. bifidum* expanded expression of LNB, galactose, GlcNAc, and central metabolism genes. Their expansion in the absence of the other is consistent with competition and niche overlap, with direct competition for the same HMO-derived carbohydrates (Fig. 7).

In contrast, *E. coli* repressed genes for fucose, NeuAc, and galactose utilization in ΔBBIF, ΔBINF, and ΔBTHE (Fig. 7 and Supplementary Information). This suggests that its ability to metabolize these sugars depends on the presence of other bacteria. *P. acidilactici* also downregulated NeuAc, GlcNAc and galactose transport upon these three dropouts, further supporting the idea that some community members rely on external activity to access specific substrates. A similar pattern emerged in ΔLSYM, where *E. coli* repressed NeuAc and central metabolism genes and *P. acidilactici* again showed broad repression. These results highlight that, beyond competition, cross-feeding and facilitation play a major role in structuring the consortium.

Beyond sugar metabolism, in ΔBBIF and ΔBINF *E. coli* repressed multiple respiratory modules, including NADH dehydrogenase complexes, cytochrome oxidases, and fumarate reductase, together with several flagellar biosynthesis genes (Fig. 7 and Supplementary Information). In parallel, genes for nitrate and nitrite reductases, lactate dehydrogenase, and quinone oxidoreductases were induced, pointing to a switch toward alternative anaerobic pathways and fermentative metabolism. This coordinated reduction of high-energy respiration and motility functions, coupled with activation of lower-energy routes, indicates a broad downshift in energy metabolism. These results suggest that in these conditions *E. coli* not only loses access to certain HMO-derived monosaccharides, but also enters a distinct physiological state characterized by reduced respiratory capacity, altered redox balance, and motility repression, potentially reflecting energy conservation. In other deletions, *E. coli* showed induction of arginine and GABA metabolism (ΔPACI, ΔLSYM), pointing to context-dependent reprogramming that extends beyond HMO utilization.

Other deletions revealed strong competitive release within the carbohydrate niches. In ΔECOL, *B. breve* markedly increased transcription of HMO utilization modules (NeuAc, fucose, GlcNAc, LNB/GNB cluster) and central metabolism genes, highlighting its overlap

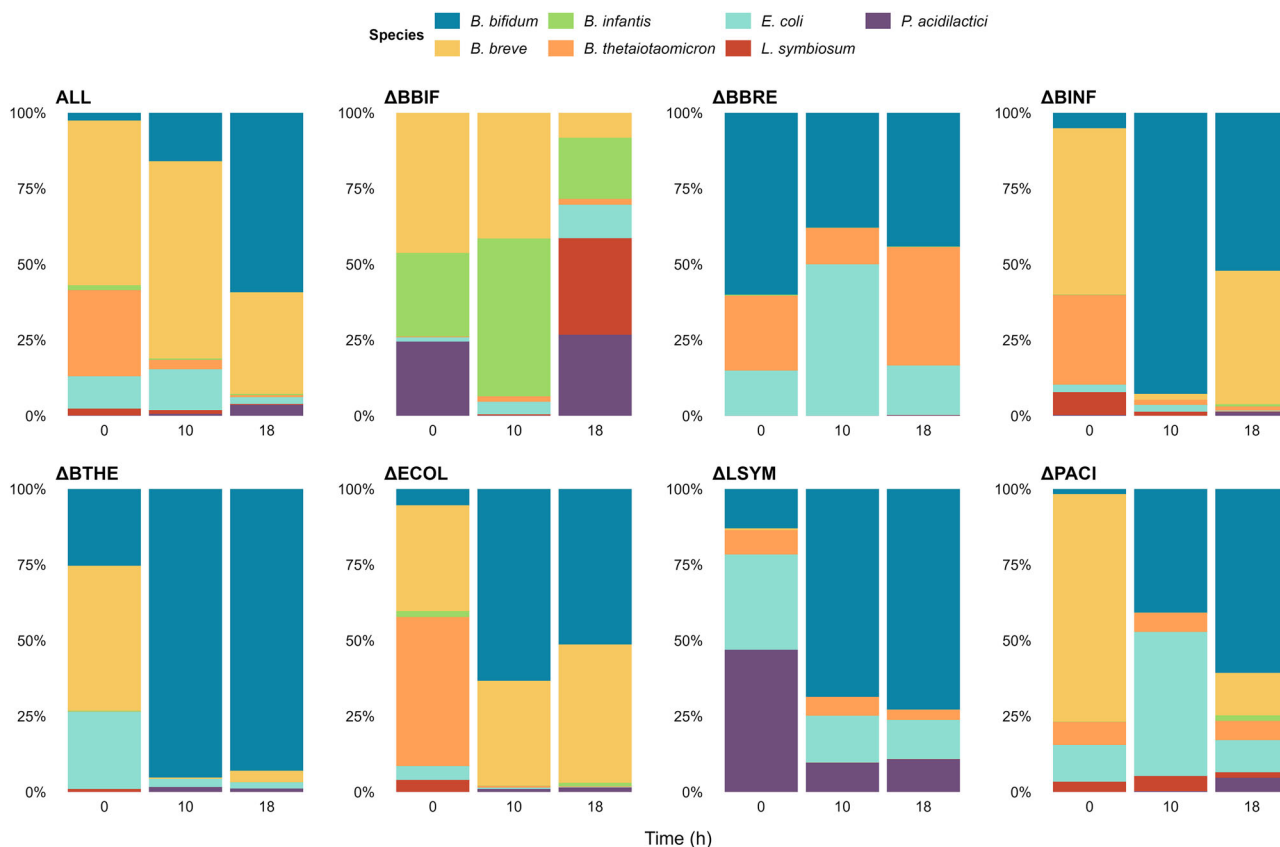


**Fig. 3 | Relative abundance of the strains used in this study.** Relative abundance of species present in each experiment at three time points: initial time (0 h), exponential growth phase (10 h), and stationary growth phase (18 h). The relative abundance was calculated using specific primers for each species by qPCR to determine the quantity of cells present. Subsequently, counting and normalization were performed, allowing the relative amount of each to be calculated.

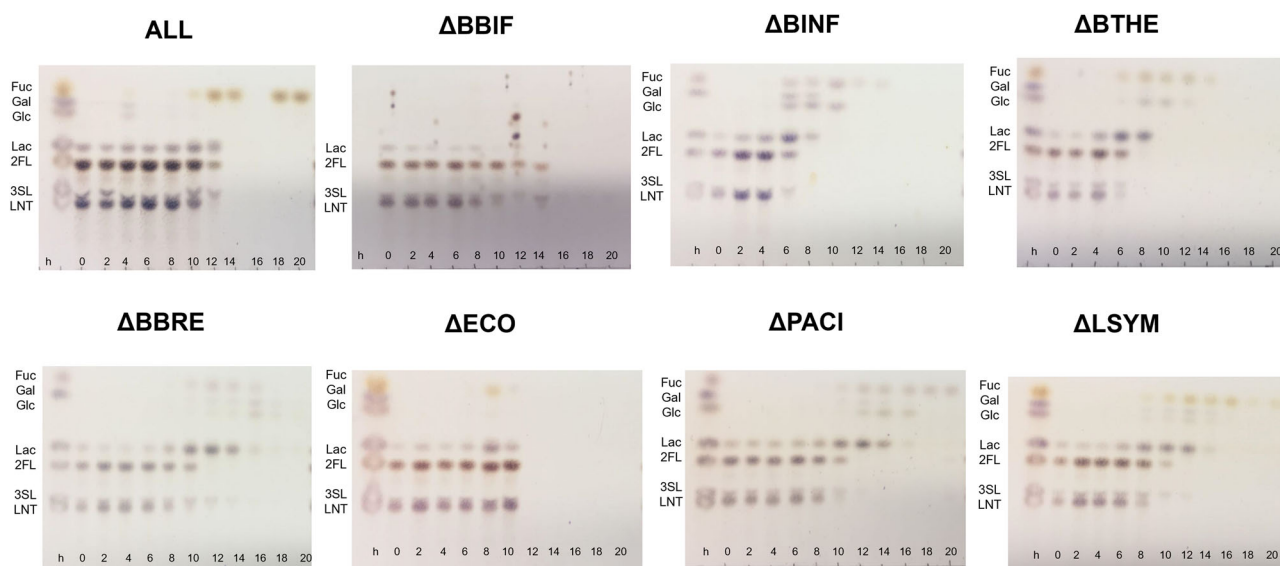


**Fig. 4 | Consumption of HMOs and derived carbohydrates for each species dropout experiment.** Thin layer chromatography (TLC) of carbohydrates of interest from experiments cultivated in mZMB with a representative mix of HMOs as carbon source. Fucose (Fuc), galactose (Gal), glucose (Glc), lactose (Lac), 2'-fucosyllactose (2'FL), 3'-sialyllactose (3'SL), and lacto-N-tetraose (LNT) were used as standards. Samples were taken every 2 h. TLCs were performed in duplicates, and the representative replicate is shown.

with *E. coli* (Fig. 7 and Supplementary Information). Similar patterns of niche expansion were observed for *B. bifidum* in ΔBINF and ΔBTHE, where galactose and GlcNAc pathways were strongly induced. *B. thetaiotaomicron* also expanded its range in ΔBBRE, upregulating fucose

and GlcNAc genes in the absence of *B. breve*. Together, these responses highlight the extent of shared metabolic niches and the rapid compensatory capacity of *Bifidobacterium* and *Bacteroides* when competitors are absent.

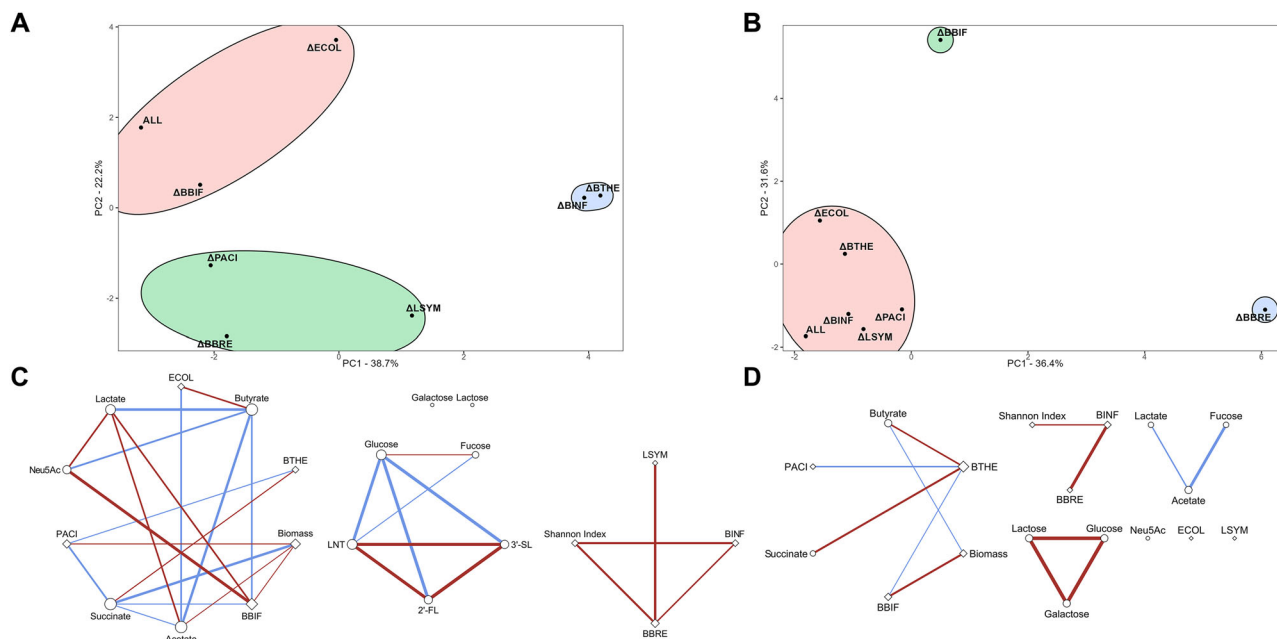
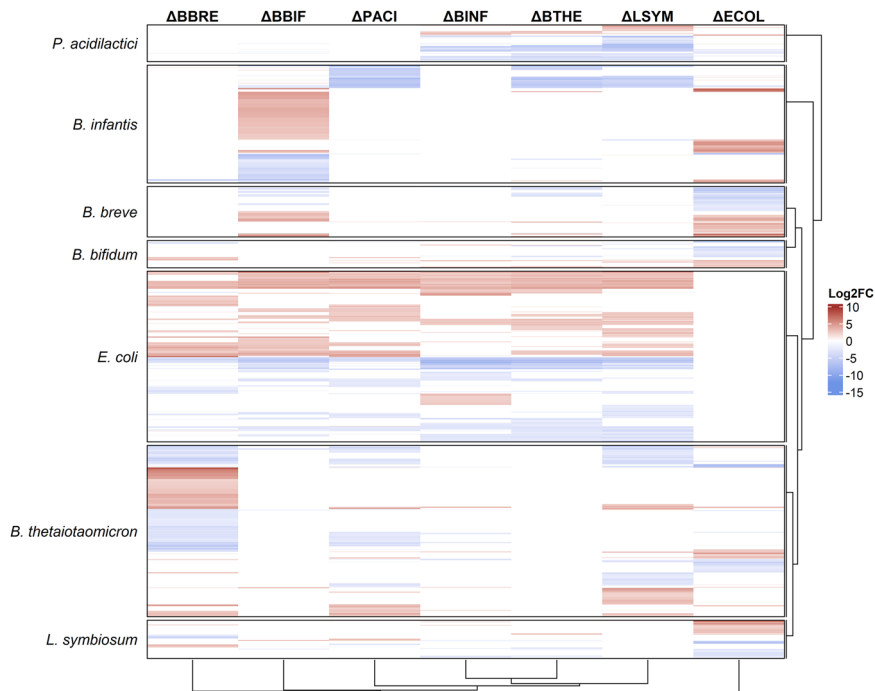


**Fig. 5 | Multivariate analyses performed in this study.** Multivariate analyses of bioreactor data. Panels display principal component analyses for exponential (A) and stationary (B) phases (10 and 18 hours, respectively), along with correlation network construction for exponential (C) and stationary (D) phases. These analyses were based on measurements of fucose, galactose, glucose, lactose, 2'FL, 3'SL, LNT, acetate, succinate, lactate, butyrate, culture absorbance, relative species abundance, and the Shannon coefficient to quantify culture diversity. The principal component analysis (A and B) shows the first two components explaining the most variability in the data (PC1 and PC2). Correlation networks (C and D) were constructed based on

the Spearman correlation coefficient, with significant interactions filtered at a 5% significance level and an absolute magnitude greater than 0.6. Burgundy-colored edges denote a positive correlation, while blue edges indicate a negative correlation. The thickness of the edge reflects the absolute magnitude of the correlation, with a thicker edge indicating a stronger correlation. The size of the node represents its degree, i.e., the number of edges connected to the node; a larger node implies a higher number of connections. Circular nodes correspond to system metabolites, while rhombus-shaped nodes are related to biomass.

**Fig. 6 | Hierarchical clustering analysis performed in this study.** Hierarchical clustering analysis was conducted using differential gene expression data for each bacterium within each experiment. The reference expression dataset consisted of the experiment containing ALL consortium. In the resulting heatmap, columns represent individual experiments, while rows correspond to specific differentially expressed genes. Genes are grouped according to their respective bacteria. The color intensity in the table reflects the expression change, quantified as Log<sub>2</sub>FC, with burgundy denoting overexpression and blue indicating repression.



**Mathematical modeling of ecological interactions in a synthetic consortium**

To further understand the dynamics of HMO degradation, we developed a system of ordinary differential equations derived from the main HMO hydrolysis reactions as in previous works (Supplementary Information<sup>45,46</sup>).

The model describes mass balances of HMO degradation and their impact on community growth.

Parameter sensitivity analysis showed that the extracellular hydrolysis constants of LNT, 2'FL, 3'SL, and lactose (k<sub>1</sub>–k<sub>4</sub>) were consistently the most influential (Fig. 8), underscoring the central role of HMO breakdown in

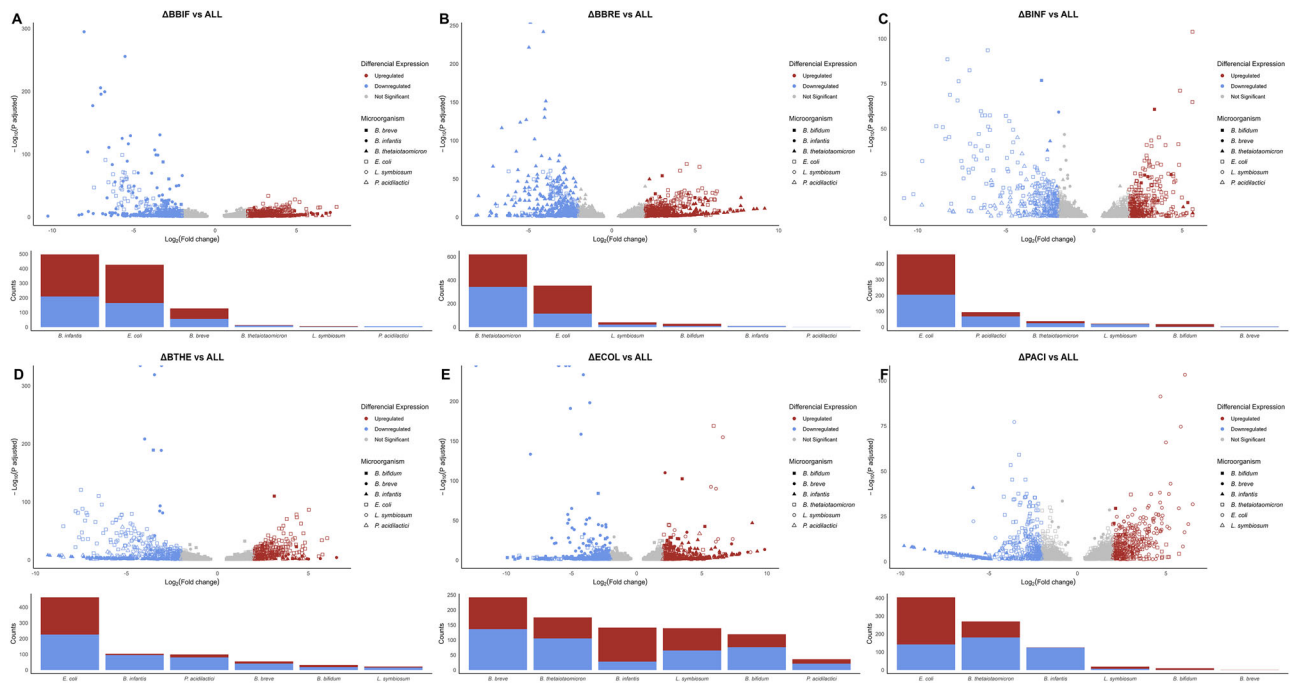


**Fig. 7 | Differential expression of specific strains in the synthetic consortium.** Visualization of differential expression of relevant bacteria in the specified consortium. In the upper panel of each panel, volcano plots with burgundy indicate overexpression, blue indicates repression, and gray denotes non-significant changes, with each point representing a gene and the shape of the point corresponding to the

microorganism on the right. Expression thresholds are marked at -2 and 2 for  $\text{Log}_2\text{FC}$  (fold change) and 0.01 for the adjusted p-value. The number of differentially expressed genes assigned to a specific bacterium is shown in the lower panel below the volcano plot. **A** ΔBBIF vs ALL; **B** ΔBBRE vs ALL; **C** ΔBINF vs ALL; **D** ΔBTHE vs ALL; **E** ΔECOL vs ALL; **F** ΔPACI vs ALL.

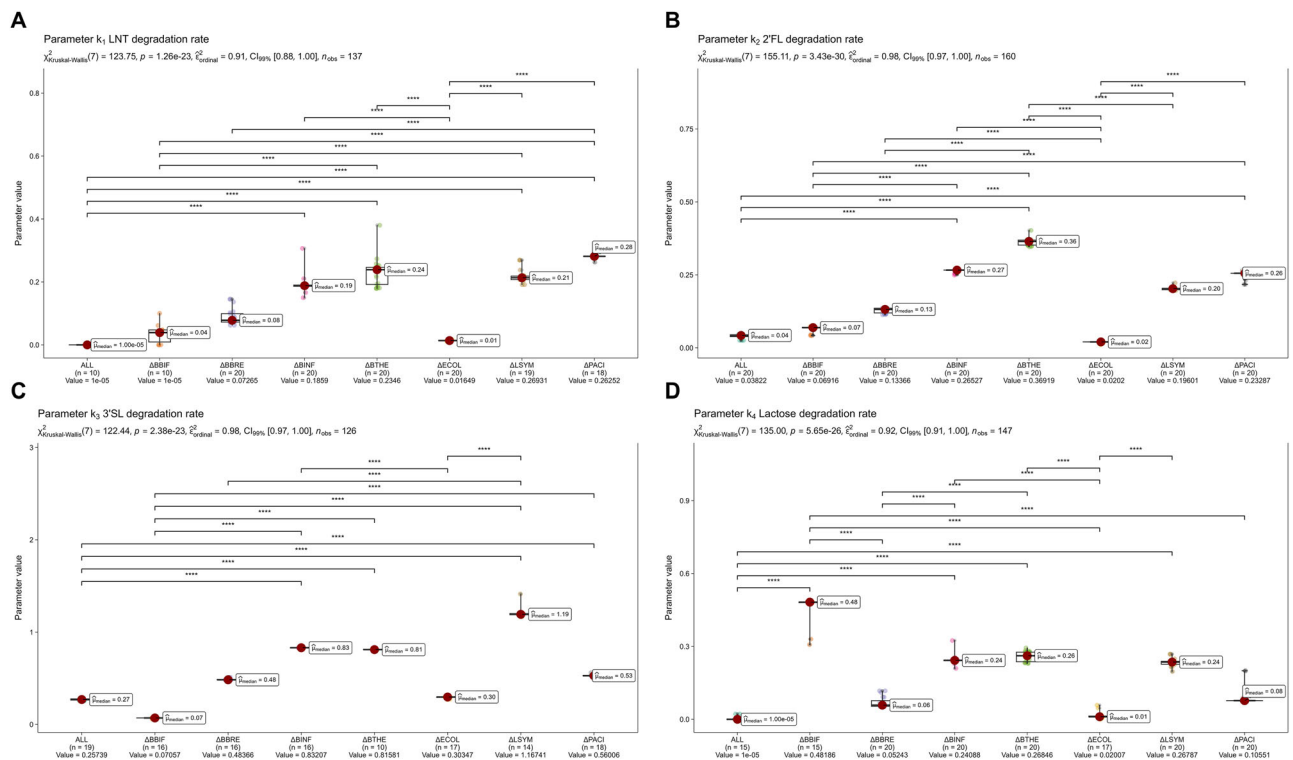


**Fig. 8 | Statistical analysis of complex oligosaccharides degradation parameters in the mathematical model.** Statistical analysis of HMO degradation parameters in the mathematical model. The degradation rate of LNT is represented by parameter  $k_1$  in the model (A), the degradation rate of 2'FL is defined by parameter  $k_2$  (B), the degradation rate of 3'SL is represented by parameter  $k_3$  (C), and the degradation rate of lactose is represented by parameter  $k_4$  (D). The statistical significance shown corresponds to adjusted p-values less than 0.0001. In the figure's subtitle, the

following values are indicated in the given order: the Chi-square statistic, the associated p-value for the statistical test, the estimated coefficient of determination of the ANOVA model, the 99% confidence interval for this coefficient value, and the total number of observations in the test. The median value of the parameter is indicated in the distributions. The experiment name is listed on the X-axis, along with the number of values in the distribution and the parameter's value in the adjusted model.

shaping consortium dynamics. The model reproduced overall growth trends and sugar consumption patterns observed experimentally, and simulations revealed that species deletions altered HMO degradation parameters. Removal of *B. bifidum* markedly reduced degradation rates across all HMOs, supporting its role as a key carbohydrate provider. In contrast, drop-outs of *B. infantis* and *B. thetaiotaomicron* accelerated HMO consumption, reflecting niche expansion and enhanced activity of *B. bifidum* in their absence.

## Discussion

Species dropouts is a valuable approach for identifying emergent roles of microbes within complex communities<sup>38</sup>. Synthetic gut microbiome consortia help determine the metabolic role of individual microorganisms and how unique strains affect gut microbiome structure and function. This approach has also been used to identify keystone species, defined as those whose disappearance causes a dramatic effect on the entire community<sup>47</sup>.

Bifidobacteria are frequent and important members of the early-life microbiota, particularly in breastfed infants in certain cohorts, and may contribute significantly to shaping the infant gut ecosystem<sup>13</sup>. HMO utilization is a crucial adaptation of bifidobacteria to the host<sup>48</sup>. *B. infantis* and *B. bifidum* share and compete for the same nutritional niche, but they are characterized by different HMO consumption mechanisms. Interestingly, both microorganisms did not adapt or modify their nutritional preferences in the presence of their competitor and did not engage in any cross-feeding interaction. The consumption mechanisms of these two archetypal bacteria also have important differences. *B. infantis* devotes a significant number of ABC transporters, multiple glycosyl hydrolases, and multiple metabolic pathways for consuming HMO and its constituents<sup>49</sup>. This strategy is energy-demanding, at least compared with *B. bifidum* extracellular degradation. *B. bifidum* has a more restricted preference for carbohydrates, mainly lactose and LNB, not metabolizing fucose or sialic acid<sup>27,50</sup>. We hypothesize that the predominance of *B. bifidum* over other competitors, especially *B. infantis* is due to its targeted strategy that probably gives this microorganism a higher growth rate on HMO under similar conditions.

Our results suggest that in this system, *B. bifidum* is a keystone species. It plays a central role in degrading HMOs, affecting community growth kinetics, and providing critical resources for the rest of the consortium. *B. bifidum* facilitates cross-feeding, leaving partially degraded HMO products<sup>51</sup>. Other studies have demonstrated a syntrophic relationship with *B. breve*, for example sharing fucose or sialic acid, which is supported by their predicted co-occurrence<sup>30,48,52</sup>. Its degradation activities can also foster the growth of other bacteria such as *Blautia wexlerae*<sup>53</sup>. Here, we also observed that *L. symbiosum* consumed NeuAc released by *B. bifidum*, and *E. coli* exploited multiple degradation products. Importantly, *B. bifidum* growth temporarily increased lactose concentration in the medium, probably derived from 2'FL and 3'SL. Most gut microbes, either commensal (such as LAB) or pathogenic bacteria, can access lactose. In contrast, *B. infantis* seems to avoid carbohydrate cross-feeding interactions with other bacteria, but acetate, lactate, and succinate produced by *B. infantis* have been involved in SCFA cross-feeding, for example, with butyrate- and propionate-producing bacteria<sup>54</sup>. The contrasting ecological consequences may have critical consequences for microbiota assembly and infant health.

Carbohydrate utilization was a dominant ecological force, driving transcriptional reprogramming upon dropouts. A recurrent observation was niche expansion: most microorganisms broadened substrate use in the absence of a competitor, revealing strong competition in this simplified model. Although *B. bifidum* showed a fitness advantage over *B. infantis* in this in vitro setting, this result contrasts with in vivo observations of some studies<sup>55</sup>. These differences likely reflect model limitations and underscore the importance of host and environmental factors in shaping microbial colonization in the infant gut.

Niche expansion was also reflected by the increased gene expression of central metabolic pathways and the activation of HMO-related metabolic pathways upon species dropouts. Microorganisms in the synthetic

consortium in this study fell into two categories: those able to access complex HMO and those using only degradation products (Fig. 8). A strong competition between *E. coli* and *B. breve* was reported here, where evidence suggested they compete for similar nutrients in the presence of *B. bifidum*. Bacterial communities in the human gut form trophic interactions<sup>56</sup>, with specialized roles in the degradation of complex polysaccharides, simple sugars, or the use of SCFA to release inorganic substrates such as CO<sub>2</sub> or H<sub>2</sub><sup>40</sup>.

Dropout experiments partially mimicked the impact of microbial extinctions in complex ecosystems such as the gut microbiome. Beneficial microbes are decreasing in modern societies<sup>5</sup>, and some *Bifidobacterium* species have shown a marked decline in prevalence, particularly in industrialized populations<sup>55</sup>. Infants in industrialized countries show a significant reduction in *B. infantis* and gene clusters associated with HMO utilization<sup>57</sup>. This phenomenon has been partly attributed to the shortening of breastfeeding in Western societies. The lack of HMO genes in their metagenomes correlates with increased inflammation and immune dysregulation, which might be related to alterations in SCFA production patterns in the infant's gut<sup>30</sup>. In turn, *B. breve* appears to be the most dominant species in industrialized infants<sup>13,57</sup>, despite being a sub-optimal HMO consumer. *B. breve* and *B. longum* have been characterized as sub-optimal HMO users in gnotobiotic mice, being outcompeted by efficient HMO consumers<sup>58</sup>. However, *B. infantis* has been associated with reduced asthma risk in antibiotic-exposed infants, while *B. breve* has shown beneficial effects on intestinal barrier maturation and immune modulation<sup>14,59</sup>. We hypothesize that a microbiome dominated by sub-optimal HMO consumers such as *B. breve* will not use the entire potential of HMO, rendering some HMOs unconsumed and being lost in infant feces. Interestingly, HMO administration permits the engraftment of *B. infantis* in adults<sup>60</sup>. This symbiotic combination increased butyrate and butyrate-producing bacteria abundance in vitro and in vivo, as well as propionate-producing bacteria in subjects undergoing antibiotic-induced dysbiosis, thereby reducing inflammatory markers<sup>54</sup>.

One important limitation of this study is the assumption that all dropouts follow a similar trajectory and that priority effects are not relevant. In microbial ecology, priority effects relate to the impact of order and the impact of species arrival in the structure of a community<sup>61</sup>. Dissimilar initial abundances (Fig. 3) might result in different final microbial compositions upon each dropout, and even in different rates or mechanisms of HMO utilization, limiting the observations of this study. Interestingly, HMO reduce significantly the impact of priority effects in vitro and in vivo<sup>62</sup>, suggesting that the deterministic force of HMO utilization overrides any initial condition of the community. Similarly, studies on priority effects on bifidobacteria show that *B. breve* benefits from fucose released from other microbes to become a dominant species<sup>63</sup>.

In addition to these ecological considerations, there are methodological limitations inherent to our experimental setup. Although each species was inoculated at OD600 = 1.0, we acknowledge that OD600 does not equate to equivalent cell numbers due to differences in cell size and optical properties, which may contribute to variability between inocula. Furthermore, traces of *E. coli* DNA were detected in the ΔECO condition by qPCR at Time 0, potentially due to residual DNA in the bioreactor system or minor cross-contamination during inoculation. However, this signal was less than 2% of total genomic DNA, and ΔECO exhibited distinct metabolic and transcriptomic profiles, suggesting minimal impact on overall community dynamics. Two strains used in this study (*B. breve* and *P. acidilactici*) are laboratory isolates under characterization for HMO utilization with no major previous history of use, whereas all other members of the consortium were well-established type strains. While strain-level variation may influence ecological interactions in vivo, we believe this simplified consortium captured key metabolic behaviors of the infant gut microbiome. The simplified nature of our synthetic consortium, the use of a single strain per species, and bioreactor-specific constraints (e.g., possible biofilm formation) also limit extrapolation of these results to the highly complex and dynamic environment of the infant gut.

In summary, these findings reveal emergent ecological roles within a synthetic infant gut community. *B. bifidum* acts as a keystone species by degrading HMOs extracellularly and releasing simple carbohydrates that support cross-feeding with other species. In contrast, species such as *B. infantis* and *B. thetaiotaomicron* compete for similar niches and primarily rely on intracellular HMO utilization. *B. breve* exhibits cooperative traits by releasing fucose, lactose, and galactose, while *E. coli* shows strong competition for HMO-derived substrates. *P. acidilactici* and *L. symbiosum* appear to be important in the consumption of lactose and NeuAc, respectively. At the community level, HMO degradation shaped competition, niche expansion, and metabolic acceleration, providing mechanistic insights into colonization dynamics in the infant gut.

## Methods

### Bacterial strains and culture media

The strains used in this study were obtained from BEI Resources, ATCC, and UC Davis Culture Collection (Table 1). For routine experiments, microorganisms were cultured in their respective media (Table 1). Luria-Bertani medium (LB; Becton, Dickinson, Franklin Lakes, NJ) was used directly, while reinforced clostridium broth (RCM; Becton, Dickinson, Franklin Lakes, NJ) and Man-Rogosa-Sharpe broth (MRS; Becton, Dickinson, Franklin Lakes, NJ) were supplemented with 0.05% w/v of L-cysteine-HCl (Sigma-Aldrich, St. Louis, MO, USA). The cultures were incubated at 37 °C for 24–48 h in an anaerobic jar (Anaerocult; Merck, Darmstadt, Germany) with anaerobic packs (Gaspak EM; Becton-Dickinson, Franklin Lakes, NJ, USA).

### Bioreactor setup and operation

Eight batch experiments were conducted in duplicate using two 250 mL bioreactors connected to a MyControl system under anaerobic conditions (Mini-bio Applikon Biotechnology, The Netherlands). The first experiment involved inoculation with the complete consortium (ALL). The remaining experiments replicated the conditions of the whole consortium but with one species each time. Therefore, each bioreactor was inoculated with six strains (Table 1). For simplicity, consortia where a given species was omitted from inoculation are referred to using the  $\Delta$  notation (e.g.,  $\Delta$ BBIF), indicating a ‘species dropout’ condition rather than an active deletion from an established community.

Before inoculation, microorganisms were cultured in modified ZMB medium<sup>64</sup> supplemented with lactose (20 g/L) at 37 °C for 24–48 h under anaerobic conditions. Microorganisms were inoculated at an OD<sub>600</sub> of 1.0 and were previously washed in fresh reduced mZMB without a carbon source. The bioreactors contained the same mZMB formulation and were supplemented with three HMOs at 2% (45% LNT, 40% 2’FL, and 15% 3’SL) (Glycom, Denmark). These values corresponded to approximate HMO concentrations in breast milk reported by Conze et al.<sup>65</sup>. The anaerobic environment inside the bioreactors was maintained using nitrogen (99.99% purity), which was injected at the beginning of the fermentation and was continuously monitored. The temperature was set to 37 °C, and the mixture was stirred at 90 rpm. The pH was maintained constant throughout the fermentation at 5.5 using an automatic injection of NaOH and HCl 3 M. Samples were taken every two hours up to 24 h and immediately centrifuged at 8000 rpm for 3 min. Pellets were stored at -80 °C and subsequently used for DNA extraction and determination of relative abundance by qPCR. In addition, another pellet was resuspended in 1 mL of RNA later (Sigma, St. Louis, MO, USA). The supernatants were used for metabolite analysis. The growth curves of the experiments were adjusted to the Gompertz-Zwietering<sup>66</sup> equation using R software, obtaining the growth parameters for each replicate. Statistical analysis of growth parameters was performed in the R package *stats*.

### DNA extraction

Genomic DNA was extracted using a modified phenol-chloroform isoamyl protocol<sup>67</sup>. Briefly, cell pellets were lysed with lysozyme and incubated at 37 °C for 30 min (Amresco, Toronto, Canada). The suspensions were

purified using phenol: chloroform: isoamyl-alcohol 25:24:1 pH 8 and sterile acid-washed-glass beads (Sigma, St. Louis, MO, USA). The cells were disrupted using Disruptor Genie for 6 min (Scientific Industries, Bohemia, NY, USA) and centrifuged for phase separation. The supernatants were purified using chloroform: isoamyl alcohol 24:1 and centrifuged for phase separation. The DNA was precipitated using isopropanol and sodium acetate 3 M. The precipitated DNA was pelleted by centrifugation, washed twice with cold ethanol, and dried by ethanol evaporation. DNA concentrations were calculated by measuring absorbance at 260 nm using an Infinite M200 PRO spectrophotometer (Tecan)<sup>51</sup>.

### Carbohydrate consumption

The total carbohydrate consumption was analyzed by Thin Layer Chromatography (TLC) using a silica gel plate F 60 (Merck, Germany). Galactose, glucose, fucose, lactose, 2’FL, 3’SL, and LNT were used as standards. 1-butanol/ethanol/water 1,75:1,25:1 v/v was used as the mobile phase, and 1%  $\alpha$ -naphthol, 0.5% sulphuric acid (5% solution) in ethanol as solvent was used as revealing solution<sup>34</sup>. 1  $\mu$ L of each sample was diluted in 2  $\mu$ L ultra-pure water, applied to the plate, dried, and run, followed by a 10 s incubation in an oven<sup>68</sup>. Numerical values were estimated using ImageJ software based on band intensity<sup>69</sup>. Sialic acid concentrations were determined using an enzymatic kit (Sigma Aldrich, Germany) according to the manufacturer’s instructions.

### High-Performance Liquid Chromatography (HPLC)

Acetic, butyric, lactic, propionic, and succinic acids from each supernatant obtained from the bioreactor experiments were quantified using a Lachrom L-700 HPLC system (Hitachi, Japan), using an Aminex HPX87H Ion exclusion column (300 mm  $\times$  7.8 mm, Bio-Rad) and an isocratic mobile phase with 5 mM H<sub>2</sub>SO<sub>4</sub><sup>70</sup>. 30  $\mu$ L of supernatant were injected at a flux of 0.45 mL/min at 35 °C for 35 min. Standard curves were obtained using nine dilutions of 30 to 0.155 g/L of each acid in HPLC-grade water. 24 conditions were tested in duplicates.

### Determination of relative bacterial abundance

Relative and absolute bacterial abundance were determined by qPCR using a set of species-specific primers based on the unique genes present in each microorganism (Supplementary Table 3). Amplification and detection were carried out using StepOnePlus equipment (Applied Biosystems, USA) in 96-well optical plates (MicroAmp Fast Optical, Thermo Fisher, USA). Briefly, 96-well plates were filled with a mixture containing 5 mL of PowerUp SYBR Master Mix or Fast SYBR Green Master Mix (Applied Biosystems, USA), 0.3 mM of each primer (0.3 mL each), 4.4 mL nuclease-free water (IDT, USA), and 1 mL of DNA (diluted to 10 ng/mL). DNA samples were amplified with an initial hold at 50 °C for 2 min and a polymerase activation step at 95 °C for 15 min for PowerUp SYBR Master Mix or 95 °C for 20 s for Fast SYBR Green Master Mix, followed by 40 cycles of denaturation at 95 °C for 10 s, annealing and elongation at 60 °C for 30 s. A melting curve was generated to verify a single amplification peak by increasing the temperature from 65 °C to 95 °C. Reactions were performed in triplicate, and threshold cycle (CT) values were converted into genome copy numbers per mL according to a previously described procedure<sup>71</sup>.

### RNA extraction and RNA gene sequencing

Pellets from 1 mL of each sample in the exponential phase were resuspended in 2 mL of RNA-later solution and stored at -80 °C. Subsequently, RNA was extracted with 1 mL of lysis buffer from the RNeasy Kit (Qiagen, MD) containing 1%  $\beta$ -mercaptoethanol (added before buffer use). The suspension was centrifuged to separate the aqueous phase from the organic phase. The aqueous layer was precipitated in ethanol, and RNA was re-dissolved in 400  $\mu$ L lysis buffer and further purified using RNeasy columns (Qiagen, MD) according to the manufacturer’s instructions. The integrity and quantity of isolated total RNA samples were determined using a high-resolution electrophoresis system (Agilent 2100 Bioanalyzer, Agilent, CA). After quality verification, samples were depleted of rRNA using the QIAseq

stranded total rRNA kit (Qiagen, MD). Libraries were prepared using the QIAseq Stranded RNA Library (Qiagen, MD) and sequenced on a NextSeq 500 Illumina at the Unidad de Genómica y Bioinformática at the University of Santiago of Chile (Santiago, Chile).

### Multivariate data analysis

Data from the exponential and stationary phases (10 and 18 h, respectively) were used for multivariate analysis. We considered the concentration of metabolites, biomass, relative abundance, and Shannon diversity coefficient<sup>72</sup>. The results were analyzed using the R software<sup>73</sup>. The *prcomp* function was used for principal component analysis (PCA), and the number of clusters was determined using the *factoextra* package<sup>74</sup>. Spearman's correlation was calculated for network construction and interactions with a significance level greater than 5% were included. Cytoscape was used for network visualization<sup>75</sup>.

### Metatranscriptomic analysis

A Jupyter notebook<sup>76</sup> was generated using the Bash kernel, detailing the step-by-step procedures. The paired library quality was assessed using FastQC<sup>77</sup> and MultiQC<sup>78</sup>, followed by quality filtering and trimming using Trimmomatic<sup>79</sup> and VSEARCH<sup>80</sup>. The mRNA reads were separated from the rRNA reads using SortMeRNA<sup>81</sup>. Reference genomes were extracted from the Bacterial and Viral Bioinformatics Resource Center (BV-BRC) database<sup>82</sup>. The following genomes were used: *Bifidobacterium bifidum* JCM 1254 (Genome ID:398514.7), *Bifidobacterium breve* DSM 20213 = JCM 1192 (Genome ID:518634.20), *Bifidobacterium longum* subsp. *infantis* ATCC 15697 = JCM 1222 (Genome ID:391904.5), *Bacteroides thetaiotaomicron* VPI-5482 (Genome ID:226186.12), *Escherichia coli* str. K-12 substr. MG1655 (Genome ID:511145.12), *Lachnospirillum symbiosum* WAL-14673 (Genome ID:742741.3), and *Pediococcus acidilactici* strain PMC65 (Genome ID:1254.353). HISAT2<sup>83</sup> was used for alignment, and file manipulation was performed using Samtools<sup>84</sup>. HTSeq<sup>85</sup> was used to generate the count matrix. PCA was conducted on the count matrix with data transformed using variance stabilization (VST) from the DESeq2 package<sup>86</sup>. For PCA, the furthest replicate was excluded, and the analysis was performed using the two closest replicates.

Taxonomic composition was estimated using SAMSA2<sup>87</sup> to identify potential outlier replicates. One replicate per treatment was removed due to compositional discrepancies confirmed by principal component analysis. Normalization of metatranscriptomic counts was performed using the taxon-specific scaling approach described by Klingenberg et al.<sup>88</sup>. Briefly, raw counts were partitioned by organism, and for each taxon a matrix was constructed that included both treatment ( $\Delta$ ) and control (ALL) replicates. Size factors and dispersions were estimated across these taxon-specific datasets using DESeq2<sup>86</sup>, ensuring that normalization reflected micro-organism transcriptional activity rather than compositional differences in community structure. Differential expression analysis was performed using the DESeq2 package with the *lfcShrink* function<sup>89</sup>. A Benjamini-Hochberg adjusted p-value  $\leq 0.01$  and a  $\log_2$  fold change  $\geq 2$  were used as filtering criteria. Volcano plots were generated with ggplot2 using the significant DESeq2 results. For each experiment,  $\log_2$  fold-change was plotted against the  $-\log_{10}$  adjusted P-value, with capped y-values to facilitate visualization of highly significant genes.

### Dynamic model

The mathematical model was based on the mass balance of the system using a system of ordinary differential equations. This model is a proprietary development that uses modified Monod kinetics for community growth (Supplementary Information). The model contained 10 differential equations, 1 algebraic equation, and 22 parameters. MATLAB software was used for modeling and parameter fitting, employing a cooperative enhanced scatter search from the MEIGO package<sup>90</sup>. The parameter-fitting procedure was as follows. A primary fit was performed with five iterations for each set of experimental data, and the set with the lowest sum of squares error (SSE) was selected. Subsequently, an identifiability analysis was conducted for

each set of experimental data to determine a set of highly sensitive parameters called “core parameters” and a set of less sensitive parameters called “shell parameters”. Once the parameter classification was determined, the core parameters were adjusted using 20 iterations, the obtained values were stored, and the set with the lowest SSE was selected. Finally, the shell parameters were adjusted using ten iterations, storing the values found and selecting the set with the lowest SSE. For statistical analysis, the values obtained for each iteration were collected, and an analysis of variance using the Kruskal-Wallis test was performed for paired comparisons. All the codes used can be found on the following Github page: [https://github.com/taproschle/msc\\_taproschle](https://github.com/taproschle/msc_taproschle).

### Data availability

Raw data and analyses are provided in the “raw data” file, Supplementary Information, and deseq results of normalized transcriptome data are found in [https://github.com/taproschle/msc\\_taproschle](https://github.com/taproschle/msc_taproschle).

### Code availability

Code and analyses are provided in the “raw data” file, supplementary information, and [https://github.com/taproschle/msc\\_taproschle](https://github.com/taproschle/msc_taproschle).

Received: 27 March 2025; Accepted: 8 November 2025;

Published online: 23 November 2025

### References

- Ahearn-Ford, S., Berrington, J. E. & Stewart, C. J. Development of the gut microbiome in early life. *Exp. Physiol.* **107**, 415–421 (2022).
- Bäckhed, F. et al. Dynamics and stabilization of the human gut microbiome during the first year of life. *Cell Host Microbe* **17**, 690–703 (2015).
- Iizumi, T. et al. Gut Microbiome and Antibiotics. *Arch. Med. Res.* **48**, 727–734 (2017).
- Homann C. M. et al. Infants' first solid foods: Impact on gut microbiota development in two intercontinental cohorts. *Nutrients* **13**, <https://doi.org/10.3390/nu13082639> (2021).
- Henrick, B. M. et al. Bifidobacteria-mediated immune system imprinting early in life. *Cell* **184**, 3884–3898.e11 (2021).
- Martin, A. J. M., Serebrinsky-Duek, K., Riquelme, E., Saa, P. A. & Garrido, D. Microbial interactions and the homeostasis of the gut microbiome: the role of Bifidobacterium. *Microbiome Res Rep* **2**, 17 (2023).
- Niñonuevo, M. R. et al. Daily variations in oligosaccharides of human milk determined by microfluidic chips and mass spectrometry. *J. Agric Food Chem.* **56**, 618–626 (2008).
- Vinjamuri, A. et al. Human Milk Oligosaccharide Compositions Illustrate Global Variations in Early Nutrition. *J. Nutr.* **152**, 1239–1253 (2022).
- Xu, G. et al. Absolute quantitation of human milk oligosaccharides reveals phenotypic variations during lactation. *J. Nutr.* **147**, 117–124 (2017).
- Thomson, P., Medina, D. A. & Garrido, D. Human milk oligosaccharides and infant gut bifidobacteria: Molecular strategies for their utilization. *Food Microbiol.* **75**, 37–46 (2018).
- Totten, S. M. et al. Comprehensive profiles of human milk oligosaccharides yield highly sensitive and specific markers for determining secretor status in lactating mothers. *J. Proteome Res.* **11**, 6124–6133 (2012).
- Casaburi, G. et al. Metagenomic insights of the infant microbiome community structure and function across multiple sites in the United States. *Sci. Rep.* **11**, 1472 (2021).
- Stewart, C. J. et al. Temporal development of the gut microbiome in early childhood from the TEDDY study. *Nature* **562**, 583–588 (2018).
- Dai, D. L. Y. et al. Breastfeeding enrichment of *B. longum* subsp. *infantis* mitigates the effect of antibiotics on the microbiota and childhood asthma risk. *Med* **4**, 92–112.e5 (2023).

15. Ferretti, P. et al. Mother-to-Infant Microbial Transmission from Different Body Sites Shapes the Developing Infant Gut Microbiome. *Cell Host Microbe*. **24**, 133–145.e5 (2018).
16. James, K. et al. Bifidobacterium breve UCC2003 metabolises the human milk oligosaccharides lacto-N-tetraose and lacto-N-neo-tetraose through overlapping, yet distinct pathways. *Sci. Rep.* **6**, 1–16 (2016).
17. Sela, D. A. et al. The genome sequence of Bifidobacterium longum subsp. infantis reveals adaptations for milk utilization within the infant microbiome. *Proc. Natl. Acad. Sci. USA* **105**, 18964–18969 (2008).
18. Yassour, M. et al. Strain-Level Analysis of Mother-to-Child Bacterial Transmission during the First Few Months of Life. *Cell Host Microbe* **24**, 146–154.e4 (2018).
19. Pichler, M. J. et al. Butyrate producing colonic Clostridiales metabolise human milk oligosaccharides and cross feed on mucin via conserved pathways. *Nat. Commun.* **11**, 3285 (2020).
20. Kijner S., Cher A., Yassour M. The Infant Gut Commensal Bacteroides dorei Presents a Generalized Transcriptional Response to Various Human Milk Oligosaccharides. *Front. Cell Infect Microbiol.* **12**, <https://doi.org/10.3389/fcimb.2022.854122> (2022).
21. Chia, L. W. et al. Bacteroides thetaiotaomicron Fosters the Growth of Butyrate-Producing Anaerostipes caccae in the Presence of Lactose and Total Human Milk Carbohydrates. *Microorganisms* **8**, 1513 (2020).
22. Zúñiga, M., Yebra, M. J. & Monedero, V. Complex Oligosaccharide Utilization Pathways in Lactobacillus. *Curr. Issues Mol. Biol* **40**, 49–80, <https://doi.org/10.21775/cimb.040.049> (2021).
23. Shani G. et al. Fucosylated Human Milk Oligosaccharide Foraging within the Species Bifidobacterium pseudocatenulatum Is Driven by Glycosyl Hydrolase Content and Specificity. *Appl. Environ. Microbiol.* **88**, <https://doi.org/10.1128/AEM.01707-21> (2022).
24. Díaz R. et al. Comparative genomic analysis of novel bifidobacterium longum subsp. Longum strains reveals functional divergence in the human gut microbiota. *Microorganisms* **9**, <https://doi.org/10.3390/microorganisms9091906> (2021).
25. Zabel, B. E. et al. Strain-specific strategies of 2'-fucosyllactose, 3-fucosyllactose, and difucosyllactose assimilation by Bifidobacterium longum subsp. infantis Bi-26 and ATCC 15697. *Sci. Rep.* **10**, 1–18 (2020).
26. Masi, A. C. & Stewart, C. J. Untangling human milk oligosaccharides and infant gut microbiome. *iScience* **25**, 103542 (2022).
27. Turrone, F. et al. Genome analysis of Bifidobacterium bifidum PRL2010 reveals metabolic pathways for host-derived glycan foraging. *Proc. Natl. Acad. Sci. USA* **107**, 19514–19519 (2010).
28. Kato, T. et al. Enzymatic adaptation of Bifidobacterium bifidum to host glycans, viewed from glycoside hydrolyases and carbohydrate-binding modules. *Microorganisms* **8**, <https://doi.org/10.3390/microorganisms8040481> (2020).
29. Garrido, D. et al. A novel gene cluster allows preferential utilization of fucosylated milk oligosaccharides in Bifidobacterium longum subsp. longum SC596. *Sci. Rep.* **6**, 1–18 (2016).
30. Tsukuda, N. et al. Key bacterial taxa and metabolic pathways affecting gut short-chain fatty acid profiles in early life. *ISME J.* **15**, 2574–2590 (2021).
31. Chia, L. W. et al. Cross-feeding between Bifidobacterium infantis and Anaerostipes caccae on lactose and human milk oligosaccharides. *Benef. Microbes* **12**, 69–83 (2021).
32. Sung, J. Global metabolic interaction network of the human gut microbiota for context-specific community-scale analysis. *Nat. Commun.* **8**, 15393 (2017).
33. Ghoul, M. & Mitri, S. The ecology and evolution of microbial competition. *Trends Microbiol* **24**, 833–845 (2016).
34. Costello, E. K. et al. The application of ecological theory toward an understanding of the human microbiome. *Science (1979)* **336**, 1255–1262 (2012).
35. Gilbert, J. A. & Lynch, S. V. Community ecology as a framework for human microbiome research. *Nat. Med* **25**, 884–889 (2019).
36. Shetty, S. A. et al. Intestinal microbiome landscaping: Insight in community assemblage and implications for microbial modulation strategies. *FEMS Microbiol Rev.* **41**, 182–199 (2017).
37. Shetty S. A. et al. Inter-species Metabolic Interactions in an In-vitro Minimal Human Gut Microbiome of Core Bacteria. *NPJ Biofilms Microbiomes* **8**, <https://doi.org/10.1038/s41522-022-00275-2> (2022).
38. Sprockett, D. D. & Coyte, K. Z. When microbes go missing: Understanding the impact of diversity loss within the gut microbiome. *Cell Host Microbe* **31**, 1249–1251 (2023).
39. Wang, M. et al. Strain dropouts reveal interactions that govern the metabolic output of the gut microbiome. *Cell* **186**, 2839–2852.e21 (2023).
40. Shetty, S. A. et al. Dynamic metabolic interactions and trophic roles of human gut microbes identified using a minimal microbiome exhibiting ecological properties. *ISME J.* **16**, 2144–2159 (2022).
41. Elzinga J. et al. The use of defined microbial communities to model host-microbe interactions in the human gut. *Microbiol. Mol. Biol. Rev.* **83**, <https://doi.org/10.1128/mmb.00054-18> (2019).
42. Morgan X. et al. Integrated culturing, modeling and transcriptomics uncovers complex interactions and emergent behavior in a three-species synthetic gut community. <https://doi.org/10.7554/eLife.37090.001> (2018).
43. Shetty, S. A., Smidt, H. & de Vos, W. M. Reconstructing functional networks in the human intestinal tract using synthetic microbiomes. *Curr. Opin. Biotechnol.* **58**, 146–154 (2019).
44. Venturelli, O. S. et al. Deciphering microbial interactions in synthetic human gut microbiome communities. *Mol. Syst. Biol.* **14**, e8157 (2018).
45. Pinto, F. et al. Modeling Metabolic Interactions in a Consortium of the Infant Gut Microbiome. *Front. Microbiol.* **8**, 2507 (2017).
46. Medina D. A. et al. Simulation and modeling of dietary changes in the infant gut microbiome. *FEMS Microbiol. Ecol.* <https://doi.org/10.1093/femsec/fiy140> (2018).
47. Gutiérrez, N. & Garrido, D. Species deletions from microbiome consortia reveal key metabolic interactions between gut microbes. *mSystems* **4**, e00185-19 (2019).
48. Walsh, C. et al. Human milk oligosaccharide-sharing by a consortium of infant derived Bifidobacterium species. *Sci. Rep.* **12**, 1–14 (2022).
49. Lawson, M. A. E. et al. Breast milk-derived human milk oligosaccharides promote Bifidobacterium interactions within a single ecosystem. *ISME J.* **14**, 635–648 (2020).
50. Garrido D. et al. Comparative transcriptomics reveals key differences in the response to milk oligosaccharides of infant gut-associated bifidobacteria. *Sci. Rep.* **5**, <https://doi.org/10.1038/srep13517> (2015).
51. Gotoh, A. et al. Sharing of human milk oligosaccharides degradants within bifidobacterial communities in faecal cultures supplemented with Bifidobacterium bifidum. *Sci. Rep.* **8**, 1–14 (2018).
52. Centanni, M. et al. Bifidobacterium bifidum ATCC 15696 and Bifidobacterium breve 24b Metabolic Interaction Based on 2' - O-Fucosyl-Lactose Studied in Steady-State Cultures in a Freter-Style Chemostat. *Appl Environ. Microbiol* **85**, 1–17 (2019).
53. Horigome A. et al. 2'-Fucosyllactose Increases the Abundance of Blautia in the Presence of Extracellular Fucosidase-Possessing Bacteria. *Front. Microbiol.* **13**, <https://doi.org/10.3389/fmicb.2022.913624> (2022).
54. Button, J. E. et al. Precision modulation of dysbiotic adult microbiomes with a human-milk-derived synbiotic reshapes gut microbial composition and metabolites. *Cell Host Microbe* **31**, 1523–1538.e10 (2023).
55. Taft, D. H. et al. Bifidobacterium Species Colonization in Infancy: A Global Cross-Sectional Comparison by Population History of Breastfeeding. *Nutrients* **14**, 1423 (2022).

56. Goyal A. et al. Ecology-guided prediction of cross-feeding interactions in the human gut microbiome. *Nat. Commun.* **12**, <https://doi.org/10.1038/s41467-021-21586-6> (2021).
57. Olm, M. R. et al. Robust variation in infant gut microbiome assembly across a spectrum of lifestyles. *Science* **376**, 1220–1223 (2022).
58. Laursen M. F., Roager H. M. Human milk oligosaccharides modify the strength of priority effects in the Bifidobacterium community assembly during infancy. *ISME J.* **2–7**(2023).
59. Preterm E. et al. Highly Specialized Carbohydrate Metabolism Capability in Bifidobacterium Strains Associated with Intestinal Barrier Maturation in Early Preterm Infants. *mBio.* **13**, e0129922, 2022, <https://doi.org/10.1128/mbio.01299-22>.
60. Button, J. E. et al. Dosing a synbiotic of human milk oligosaccharides and B. infantis leads to reversible engraftment in healthy adult microbiomes without antibiotics. *Cell Host Microbe* **30**, 712–725.e7 (2022).
61. Sprockett, D., Fukami, T. & Relman, D. A. Role of priority effects in the early-life assembly of the gut microbiota. *Nat. Rev. Gastroenterol. Hepatol.* **15**, 197–205 (2018).
62. Laursen, M. F. & Roager, H. M. Human milk oligosaccharides modify the strength of priority effects in the Bifidobacterium community assembly during infancy. *ISME J.* **17**, 2452–2457 (2023).
63. Ojima, M. N. et al. Priority effects shape the structure of infant-type Bifidobacterium communities on human milk oligosaccharides. *ISME J.* **16**, 2265–2279 (2022).
64. Medina, D. A. et al. Prebiotics mediate microbial interactions in a consortium of the infant gut microbiome. *Int J. Mol. Sci.* **18**, 1–16 (2017).
65. Conze, D. B. et al. Weighted analysis of 2'-fucosyllactose, 3-fucosyllactose, lacto-N-tetraose, 3'-sialyllactose, and 6'-sialyllactose concentrations in human milk. *Food Chem. Toxicol.* **163**, 112877 (2022).
66. Zwietering, M. H., Jongenburger, I., Rombouts, F. M., & van 't Riet, K. Modeling of the bacterial growth curve. *Appl Environ Microbiol* **56**, 1875–1881 (1990).
67. Anahtar, M. N., Bowman, B. A. & Kwon, D. S. Efficient nucleic acid extraction and 16s rRNA gene sequencing for bacterial community characterization. *J. Visualized Exp.* **2016**, 1–11 (2016).
68. Tuomivaara, S. T. et al. Generation and structural validation of a library of diverse xyloglucan-derived oligosaccharides, including an update on xyloglucan nomenclature. *Carbohydr. Res* **402**, 56–66 (2015).
69. Schneider, C. A., Rasband, W. S. & Eliceiri, K. W. NIH Image to ImageJ: 25 years of image analysis. *Nat. Methods* **9**, 671–675 (2012).
70. Mendoza, S. N. et al. Genome-scale reconstruction of the metabolic network in *Oenococcus oeni* to assess wine malolactic fermentation. *Front. Microbiol.* **8**, 1–16 (2017).
71. Medina, D. A. et al. Distinct patterns in the gut microbiota after surgical or medical therapy in obese patients. *PeerJ* **5**, 1–22 (2017).
72. Spellerberg, I. F. & Fedor, P. J. A tribute to Claude-Shannon (1916–2001) and a plea for more rigorous use of species richness, species diversity and the 'Shannon-Wiener' Index. *Glob. Ecol. Biogeogr.* **12**, 177–179 (2003).
73. Team RC. R: A language and environment for statistical computing. Vienna: R foundation for statistical computing (2021).
74. Kassambara A. Factoextra: extract and visualize the results of multivariate data analyses. *R package version;* **1**(2016).
75. Shannon, P. et al. Cytoscape: A software Environment for integrated models of biomolecular interaction networks. *Genome Res* **13**, 2498–2504 (2003).
76. Kluyver, T. et al. Jupyter Notebooks—a publishing format for reproducible computational workflows. *Elpub* **2016**, 87–90 (2016).
77. Andrews S. et al. FastQC. 2012. Babraham, UK, 2012.
78. Ewels, P. et al. MultiQC: Summarize analysis results for multiple tools and samples in a single report. *Bioinformatics* **32**, 3047–3048 (2016).
79. Bolger, A. M., Lohse, M. & Usadel, B. Trimmomatic: A flexible trimmer for Illumina sequence data. *Bioinformatics* **30**, 2114–2120 (2014).
80. Rognes, T. et al. VSEARCH: A versatile open source tool for metagenomics. *PeerJ* **2016**, 1–22 (2016).
81. Kopylova, E., Noé, L. & Touzet, H. SortMeRNA: Fast and accurate filtering of ribosomal RNAs in metatranscriptomic data. *Bioinformatics* **28**, 3211–3217 (2012).
82. Olson, R. D. et al. Introducing the Bacterial and Viral Bioinformatics Resource Center (BV-BRC): a resource combining PATRIC, IRD and ViPR. *Nucleic Acids Res.* **51**, D678–D689 (2023).
83. Kim, D. et al. Graph-based genome alignment and genotyping with HISAT2 and HISAT-genotype. *Nat. Biotechnol.* **37**, 907–915 (2019).
84. Danecek, P. et al. Twelve years of SAMtools and BCFtools. *Gigascience* **10**, 1–4 (2021).
85. Anders, S., Pyl, P. T. & Huber, W. HTSeq-A Python framework to work with high-throughput sequencing data. *Bioinformatics* **31**, 166–169 (2015).
86. Love, M. I., Huber, W. & Anders, S. Moderated estimation of fold change and dispersion for RNA-seq data with DESeq2. *Genome Biol.* **15**, 1–21 (2014).
87. Westreich, S. T. et al. SAMSA2: a standalone metatranscriptome analysis pipeline. *BMC Bioinforma.* **19**, 175 (2018).
88. Klingenberg, H. & Meinicke, P. How to normalize metatranscriptomic count data for differential expression analysis. *PeerJ* **5**, e3859 (2017).
89. Zhu, A., Ibrahim, J. G. & Love, M. I. Heavy-Tailed prior distributions for sequence count data: Removing the noise and preserving large differences. *Bioinformatics* **35**, 2084–2092 (2019).
90. Egea, J. A. et al. MEIGOR: a software suite based on metaheuristics for global optimization in systems biology and bioinformatics Continuous and mixed-integer problems. *Enhanced Scatter Search* **15**, 1–33 (2014).
91. Kiyohara, M. et al. An exo- $\alpha$ -sialidase from bifidobacteria involved in the degradation of sialyloligosaccharides in human milk and intestinal glycoconjugates. *Glycobiology* **21**, 437–447 (2011).
92. Takane, K. et al. Molecular Cloning and Characterization of Bifidobacterium bifidum 1,2- $\alpha$ -l-Fucosidase (AfcA), a Novel Inverting Glycosidase (Glycoside Hydrolase Family 95). *J. Bacteriol.* **186**, 4885–4893 (2004).
93. Jun, W. et al. Bifidobacterium bifidum Lacto-N-Biosidase, a Critical Enzyme for the Degradation of Human Milk Oligosaccharides with a Type 1 Structure. *Appl Environ. Microbiol* **75**, 6414 (2009).
94. Sela, D. A. et al. The genome sequence of Bifidobacterium longum subsp. infantis reveals adaptations for milk utilization within the infant microbiome. *Proc. Natl. Acad. Sci.* **105**, 18964–18969 (2008).
95. Sela D. A. et al. Bifidobacterium longum subsp. infantis ATCC 15697  $\alpha$ -fucosidases are active on fucosylated human milk oligosaccharides. *Appl. Environ. Microbiol* **78**, <https://doi.org/10.1128/AEM.06762-11>(2012).
96. Garrido D., Ruiz-Moyano S., Mills D. A. Release and utilization of N-acetyl-d-glucosamine from human milk oligosaccharides by Bifidobacterium longum subsp. infantis. *Anaerobe* **18**, <https://doi.org/10.1016/j.anaerobe.2012.04.012>(2012).
97. James, K. et al. Bifidobacterium breve UCC2003 metabolises the human milk oligosaccharides lacto-N-tetraose and lacto-N-neo-tetraose through overlapping, yet distinct pathways. *Sci. Rep.* **6**, 38560 (2016).
98. Ward, R. E. et al. In vitro fermentability of human milk oligosaccharides by several strains of bifidobacteria. *Mol. Nutr. Food Res.* **51**, 1398–1405 (2007).

99. Muireann, E. et al. Metabolism of Sialic Acid by *Bifidobacterium breve* UCC2003. *Appl Environ. Microbiol.* **80**, 4414–4426 (2014).
100. Chia, L. W. et al. *Bacteroides thetaiotaomicron* Fosters the Growth of Butyrate-Producing *Anaerostipes caccae* in the Presence of Lactose and Total Human Milk Carbohydrates. *Microorganisms* **8**, 2020 (2020).
101. Marcobal, A. et al. *Bacteroides* in the Infant Gut Consume Milk Oligosaccharides via Mucus-Utilization Pathways. *Cell Host Microbe* **10**, 507–514 (2011).
102. Plumbridge, J. A. Repression and induction of the nag regulon of *Escherichia coli* K-12: the roles of nagC and nagA in maintenance of the uninduced state. *Mol. Microbiol.* **5**, 2053–2062 (1991).
103. Vimr, E. R. & Troy, F. A. Identification of an inducible catabolic system for sialic acids (nan) in *Escherichia coli*. *J. Bacteriol.* **164**, 845–853 (1985).
104. Jacqueline, P. & Eric, V. Convergent Pathways for Utilization of the Amino Sugars N-Acetylglucosamine, N-Acetylmannosamine, and N-Acetylneuraminic Acid by *Escherichia coli*. *J. Bacteriol.* **181**, 47–54 (1999).

### Acknowledgements

We thank Belen Hirmas, Lucas Lagos and Benjamin Guzman for their contribution to this study. This work was supported by Fondecyt EQM190070, Fondecyt Regular 1230764, Fondecyt Exploración 13250023, SeedFund Ingeniería UC 2020 and Centro Ciencia & Vida, FB210008.

### Author contributions

T.P.D. formulated the mathematical model, performed statistical analyses and drafted the manuscript. J.V.D., K.S., I.P.S., and R.D. conducted experiments and analysis. D.G., A.J.M., R.D., J.V.D., and T.P.D. edited the manuscript. All authors discussed the data and contributed to the completion of the final manuscript.

### Competing interests

The authors declare no competing interests.

### Additional information

**Supplementary information** The online version contains supplementary material available at <https://doi.org/10.1038/s41522-025-00865-w>.

**Correspondence** and requests for materials should be addressed to Daniel Garrido.

**Reprints and permissions information** is available at <http://www.nature.com/reprints>

**Publisher's note** Springer Nature remains neutral with regard to jurisdictional claims in published maps and institutional affiliations.

**Open Access** This article is licensed under a Creative Commons Attribution-NonCommercial-NoDerivatives 4.0 International License, which permits any non-commercial use, sharing, distribution and reproduction in any medium or format, as long as you give appropriate credit to the original author(s) and the source, provide a link to the Creative Commons licence, and indicate if you modified the licensed material. You do not have permission under this licence to share adapted material derived from this article or parts of it. The images or other third party material in this article are included in the article's Creative Commons licence, unless indicated otherwise in a credit line to the material. If material is not included in the article's Creative Commons licence and your intended use is not permitted by statutory regulation or exceeds the permitted use, you will need to obtain permission directly from the copyright holder. To view a copy of this licence, visit <http://creativecommons.org/licenses/by-nc-nd/4.0/>.

© The Author(s) 2025